Microscopic calculations of the excitation spectrum of one ^{3}He impurity in liquid ^{4}He

A. Fabrocini*
Department of Physics and Material Research Laboratory, University of Illinois at Urbana-Champaign, Urbana, Illinois 61801

S. Fantoni and S. Rosati
Dipartimento di Fisica and Istituto Nazionale di Fisica Nucleare, Università di Pisa, I-56100 Pisa, Italy

A. Polls
Departament de Fisica Teorica, Universitat de Barcelona, 08028-Barcelona, Spain
(Received 16 September 1985)

We calculate the chemical potential ϵ_0 and the effective mass m^*/m_3 of one ^{3}He impurity in liquid ^{4}He. First a variational wave function including two- and three-particle dynamical correlations is adopted. Triplet correlations bring the computed values of ϵ_0 very close to the experimental results. The variational estimate of m^*/m_3 includes also backflow correlations between the ^{3}He atom and the particles in the medium. Different approximations for the three-particle distribution function give almost the same values for m^*/m_3. The variational approach underestimates m^*/m_3 by $\sim 10\%$ at all of the considered densities. Correlated-basis perturbation theory is then used to improve the wave function to include backflow around the particles of the medium. The perturbative series built up with one-phonon states only is summed up to infinite order and gives results very close to the variational ones. All the perturbative diagrams with two independent phonons have then been summed to compute m^*/m_3. Their contribution depends to some extent on the form used for the three-particle distribution function. When the scaling approximation is adopted, a reasonable agreement with the experimental results is achieved.

I. INTRODUCTION

Dilute solutions of ^{3}He atoms in superfluid ^{4}He are suitable systems to study the elementary excitations of quantum fluids. The theory is based on the properties of isolated ^{3}He atoms in the liquid, and one is allowed to describe the low-lying excited states of the system in terms of weakly interacting elementary excitations above the ground state.[1,2] There are two types of excitations: phonon and roton excitations of the ^{4}He medium, which are affected very little by the presence of ^{3}He atoms, and the ^{3}He quasiparticle excitations, characterized by the Landau-Pomeranchuck[3] spectrum

$$\epsilon_p = \epsilon_0 + p^2/2m^* , \tag{1.1}$$

where $\mathbf{p}$ is the momentum of the excitation and m^* is the quasiparticle effective mass. There is very little admixture between the two types of excitations at low momenta $p \ll m_4 c$, where $c = 238$ m/s is the ^{4}He first-sound velocity and m_4 is the mass of the ^{4}He atom.

In this paper we present and discuss a microscopic calculation of the excitation spectrum ϵ_p of *one* ^{3}He atom immersed in a background of liquid ^{4}He, determined by the two parameters ϵ_0 and m^* of Eq. (1.1). Experimentally, ϵ_0 is measured from the heat of mixing[4] of ^{3}He in ^{4}He and is $\epsilon_0 \cong -2.785$ K. The value $m^*/m_3 \cong 2.3$ for the effective mass at zero pressure has been derived from the specific heat[5] of dilute solutions and, more recently, confirmed by second-sound measurements.[6] The main reason for m^* to be ~ 2.3 times the bare mass m_3, as first proposed by Feynman and Cohen,[7] is the presence of backflow correlations between the ^{3}He impurity and the background of ^{4}He atoms.

A number of variational calculations[8–10] have been performed for the effective mass, by using a trial wave function of the type

$$\Psi_v(\mathbf{p}) = \Psi_0 F_B \exp(i\mathbf{p}\cdot\mathbf{r}_i) , \tag{1.2}$$

where Ψ_0 is the ground-state function of the ^{4}He medium plus one ^{3}He atom, and the correlation operator

$$F_B = \prod_{i=1}^{A} f_B(\mathbf{p}, \mathbf{r}_{iI}) , \tag{1.3}$$

induces backflow correlations between the impurity I (^{3}He atom) and the A atoms of the medium. The results obtained depend, to a certain extent, on the correlation functions adopted, as well as on the approximations used to evaluate the two- and three-particle distribution functions. Owen[10] assumed to have the optimal Jastrow wave function of the type

$$F_J = \prod_{\substack{i,j=1 \\ (i<j)}}^{A} e^{-u_{ij}/2} \prod_{i=1}^{A} e^{-u_{iI}/2} , \tag{1.4}$$

for Ψ_0 in Eq. (1.2) and used the optimal two-body back-

flow function $f_B(\mathbf{p},\mathbf{r}_{Ii})$. The results obtained indicate that the Feynman-Cohen effect alone is not sufficient to explain fully the enhancement of m^*/m_3 above unity. In fact the values obtained in Ref. 10 for the Lennard-Jones (LJ) potential range from 1.4 to 1.65 depending on the approximation used to calculate the three-particle distribution functions.

Triplet correlations have been found to play an important role in the binding energy per particle of ^{4}He (Ref. 11). The most reliable variational calculations[12] of the chemical potential ϵ_0 given in Eq. (1.1) use a ground-state wave function of the type

$$\Psi_0 = F_J F_T \ , \tag{1.5}$$

where the triplet correlation operator is given by

$$F_T = \prod_{\substack{i,j,k=1 \\ (i<j<k)}}^{A} e^{-q_{ijk}/2} \prod_{\substack{i,j=1 \\ (i<j)}}^{A} e^{-q_{Iij}/2} \ , \tag{1.6}$$

with

$$q_{\alpha jk} = \sum_{\text{cyc}} \zeta(r_{\alpha j})\zeta(r_{\alpha k})\hat{\mathbf{r}}_{\alpha j}\cdot\hat{\mathbf{r}}_{\alpha k} \ . \tag{1.7}$$

Here, $\sum_{\text{cyc}}$ denotes a summation on the cyclic permutations of the indices α,j,k, and the index α may represent either a ^{4}He atom or the ^{3}He impurity.

It is found that three-particle correlations, in spite of their large effect on ϵ_0,[12] give very little contribution to the variational estimate of m^*. Our best variational result, obtained by using the hypernetted-chain plus scaling (HNC/s) approximation[13,11,12] and by including two-particle correlations only, gives $m^*=1.48m_3$ at the equilibrium density $\rho_0=0.021\,85$ Å^{-3}, which is in fair agreement with the corresponding result of Ref. 10. The inclusion of triplet correlations brings the value of m^* to $1.46m_3$.

Other processes, like those by which the ^{4}He atoms acquire an effective mass, could be relevant as suggested by the recent results of Manousakis and Pandharipande[14] on the excitation spectrum of liquid ^{4}He. A different approach to study the excitation spectrum of one ^{3}He atom embedded in a liquid-^{4}He medium is furnished by the perturbation theory[15–17] based on a set of nonorthogonal correlated basis functions (CBF's) $|\Psi_i(\mathbf{p})\rangle$. These functions differ among themselves in the partition of momentum between the ^{4}He medium and the impurity ^{3}He, and are given by

$$|\Psi_i(\mathbf{p})\rangle = |\mathbf{k};\mathbf{q}_1^{m_1}\mathbf{q}_2^{m_2}\cdots\rangle = \prod_i [\rho(\mathbf{q})]^{m_i}\rho_I(\mathbf{k})\Psi_0 \ , \tag{1.8}$$

where

$$\rho(\mathbf{q}) = \sum_{i=1}^{A} e^{i\mathbf{q}\cdot\mathbf{r}_i} \ , \tag{1.9}$$

$$\rho_I(\mathbf{k}) = e^{i\mathbf{k}\cdot\mathbf{r}_I} \ . \tag{1.10}$$

In this scheme the unperturbed state is given by

$$\Psi_0(\mathbf{p}) = \rho_I(\mathbf{p})\Psi_0 \ , \tag{1.11}$$

which differs from $\Psi_v(\mathbf{p})$ of Eq. (1.2) because of the absence of the backflow operator F_B in (1.11). The inclusion of the one-phonon state $|\mathbf{k};\mathbf{p}-\mathbf{k}\rangle$ admixture in the unperturbed state $\Psi_0(\mathbf{p})$ gives most of the backflow correlation effects.[15,16] It is found that the sum of all of the perturbative terms built up with one-phonon intermediate states only (ladders) leads to a value of the effective mass $m^*=1.54m_3$ [at $\rho=\rho_0$ for the Lennard-Jones (LJ) potential], which is very close to the variational estimate.

In order to explain the excitation spectrum ϵ_p one has to go beyond second-order perturbation theory with a one-phonon intermediate state (OIP). Terms having two independent phonons (TIP) are important in explaining the discrepancy between the experimental and the theoretical estimates of m^*. These terms, as already pointed out by Woo *et al.*,[17] include the effects of the backflow correlations around the ^{4}He atoms. A large cancellation is present amongst the TIP terms, which have then *all* to be summed. The net result depends on the approximation used to calculate the three-particle distribution functions. In the best approximation used, the effective mass is $2.0m_3$ for the LJ potential and $2.2m_3$ for the Aziz potential,[18] which are quite close to the experimental value of $2.3m_3$. The contribution of the TIP terms is $\lesssim 20\%$ of the OIP term. The rapid convergence of the nIP series in the ladder-type terms strongly indicates that one should expect a similar convergence in the full nIP series. Analogous indications are furnished by the results obtained at densities higher than the equilibrium.

The paper is organized as follows. After the Introduction, Sec. II deals with variational calculations and the prescriptions for Ψ_0. The perturbative scheme for the excitation spectrum ϵ_p which has been developed in Ref. 19 will be briefly reviewed in Sec. III, where the calculation of diagonal and off-diagonal matrix elements is also treated. The results obtained for the effective mass when the ladder-type terms are included in the calculation and those provided by the OIP and TIP terms, are presented and discussed in Sec. IV.

II. VARIATIONAL CALCULATIONS

In this section we calculate the excitation spectrum ϵ_p of one ^{3}He impurity in a liquid-^{4}He medium by using the variational theory with a wave function $\Psi_v(\mathbf{p})$ of the type given in Eqs. (1.2) and (1.3) and Ψ_0 given by Eqs. (1.5)–(1.7). The correlation operators F_J and F_T, obtained by minimizing the ground-state energy E_0^v, will also be used in the perturbative calculation of m^*, discussed in the next sections, to determine Ψ_0 in the definition of the correlated-basis functions of Eq. (1.8).

The Hamiltonian of the system is given by

$$H = H_4 + H_I \ , \tag{2.1}$$

where

$$H_4 = -\frac{\hbar^2}{2m_4}\sum_{i=1}^{A}\nabla_i^2 + \sum_{\substack{i,j=1 \\ (i<j)}}^{A} v(r_{ij}) \ , \tag{2.2}$$

is the Hamiltonian of the ^{4}He background, and

$$H_I=-\frac{\hbar^2}{2m_3}\nabla_I^2+\sum_{i=1}^{A}v(r_{Ii})\ , \tag{2.3}$$

is the part which involves the impurity ^{3}He.

A. Ground state

It is convenient to write the expectation value of the Hamiltonian H with respect to Ψ_0 in the following form:

$$E_0^v=E_4^v+\epsilon_0^v\ . \tag{2.4}$$

Here E_4^v is the energy of the medium and therefore proportional to A, whereas ϵ_0^v is the chemical potential of the ^{3}He atom and hence of order of unity. The derivations of the expressions for E_4^v and ϵ_0^v have been given in Refs. 11 and 12, respectively, and will not be repeated. The expressions obtained within the Jackson-Feenberg prescription for the kinetic energy expectation value are

$$E_4^v/A=(\rho/2)\int d\mathbf{r}_{ij}g_{2,ij}\left[v_{ij}+\frac{\hbar^2}{4m_4}\nabla^2u_{ij}\right]+\frac{\hbar^2}{16m_4}\rho^2\int d\mathbf{r}_{ij}\,d\mathbf{r}_{ik}g_{3,ijk}\nabla_i^2q_{ijk}\ , \tag{2.5}$$

$$\epsilon_0^v=\epsilon_I+\epsilon_R\ , \tag{2.6}$$

where the interaction term ϵ_I is given by

$$\epsilon_I=\rho\int d\mathbf{r}_{Ij}g_{2,Ij}\left[v_{Ij}+\frac{\hbar^2}{4\mu_2}\nabla^2u_{Ij}\right]+\frac{\hbar^2}{8\mu_3}\rho^2\int d\mathbf{r}_{Ij}d\mathbf{r}_{Ik}g_{3,Ijk}\nabla_I^2q_{Ijk}\ , \tag{2.7}$$

with $1/\mu_2=\frac{1}{2}(1/m_4+1/m_3)$ and $1/\mu_3=\frac{1}{2}(2/m_4+1/m_3)$. The term ϵ_R is due to rearrangement of the medium and it is given by

$$\epsilon_R=\tfrac{1}{2}\rho^2\int d\mathbf{r}_{ij}g_{2,ij}^R\left[v_{ij}+\frac{\hbar^2}{4m_4}\nabla^2u_{ij}\right]+\frac{\hbar^2}{16m_4}\rho^3\int d\mathbf{r}_{ij}\,d\mathbf{r}_{ik}g_{3,ijk}^R\nabla_i^2q_{ijk}\ . \tag{2.8}$$

The distribution functions involved in the above equations are defined by the following equations:

$$g_{n,12\cdots n}+\frac{1}{\Omega}g_{n,12\cdots n}^R=\frac{A(A-1)\cdots(A-n+1)}{\rho^n}\frac{\int d\mathbf{r}_{n+1}\cdots|\Psi_0|^2}{\int d\tau|\Psi_0|^2}\ , \tag{2.9}$$

$$g_{n,I23\cdots n}=\frac{\Omega A(A-1)\cdots(A-n+2)}{\rho^{n-1}}\frac{\int d\mathbf{r}_{n+1}\cdots|\Psi_0|^2}{\int d\tau|\Psi_0|^2}\ . \tag{2.10}$$

In Eq. (2.9) $g_{n,12\cdots n}$ is the n-body distribution function of the medium, i.e., that obtained by setting $u_{Ij}=q_{Ijk}=0$ in Ψ_0; $(1/\Omega)g_n^R$ is the contribution to the distribution function coming from the rearrangement of the medium due to the presence of the impurity. The cluster expansions of g_{ij}, g_{Ij}, and g_{ij}^R have been extensively studied[11,12,20] and some of the contributing diagrams are displayed in Fig. 1. The two-body distribution functions are most conveniently expressed by the following equations:

$$g_{\mu j}=\exp(-u_{\mu j}+N_{\mu j}+C_{\mu j}+E_{\mu j})\,|_{\rho_I=0}\ , \tag{2.11}$$

$$g_{ij}^R=\frac{\partial}{\partial\rho_I}g_{ij}\,|_{\rho_I=0}\ , \tag{2.12}$$

where $N_{\mu j}$ and $C_{\mu j}$ are the contributions from nodal diagrams and dressed three-body links, and $E_{\mu j}=\sum_{n(\geq 4)}E_{\mu j}^{(n)}$ is the sum of the elementary diagrams. The index μ in Eq. (2.11) may represent either a ^{4}He or a ^{3}He atom. The functions N and C are calculated by solving the following integral equations of the HNC type:

$$N_{\mu j}=\sum_\nu\rho_\nu\int d\mathbf{r}_\nu(g_{\mu\nu}-1)(g_{\nu j}-N_{\nu j}-1)\ , \tag{2.13}$$

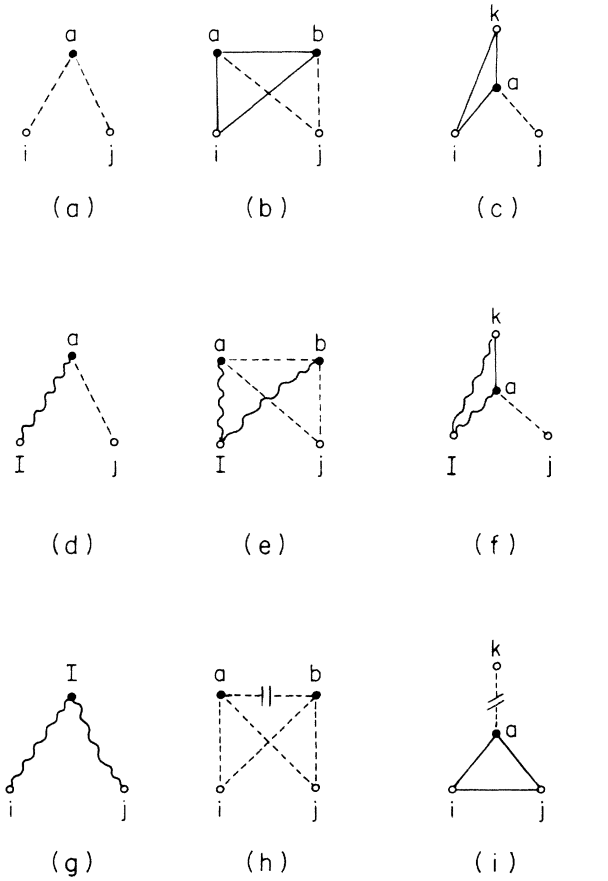

FIG. 1. HNC diagrams contributing the distribution functions. Diagrams (a)–(c) belong to g_{ij}, (d)–(f) belong to g_{Ij}, and (g)–(i) belong to g_{ij}^R. The dashed, wavy, and broken-dashed lines represent $g_{ij}-1$, $g_{Ij}-1$, and g_{ij}^R links, respectively, whereas the triangles made up of solid or wavy lines denote triplet correlations.

$$C_{\mu j}=\sum_{\nu}\rho_{\nu}\int d\mathbf{r}_{\nu}[\exp(-q_{\mu j\nu})-1]g_{\mu\nu}g_{\nu j}\ , \tag{2.14}$$

where the sum $\sum_{\nu}$ is extended over the two types of atoms in the system.

The three-body distribution functions are given by

$$g_{3,\mu jk}=g_{\mu j}g_{\mu k}g_{jk}\exp(-q_{\mu jk}+A_{\mu jk})\,|_{\rho_I=0}\ , \tag{2.15}$$

$$g^{R}_{3,ijk}=\frac{\partial}{\partial\rho_I}g_{3,ijk}\,|_{\rho_I=0}\ , \tag{2.16}$$

where $A_{\mu jk}=\sum_{n(\geq 4)}A^{(n)}_{\mu jk}$ is the sum of the Abe diagrams.[21] Both the elementary and the Abe diagrams are built up with $g-1$ links and triplet correlations and give a substantial contribution to the distribution functions.

We use the scaling approximation of Ref. 11 to calculate E and A, by taking the same scaling factors for all three types of elementary and Abe diagrams. This is justified by the fact that we keep $q_{ijk}=q_{Ijk}$ in the calculation and that g_{ij} differs very little from g_{Ij}.[12]

The correlation functions u and q appearing in Eqs. (1.4) and (1.6) are obtained by minimizing E^{v}_{4}/A and then ϵ^{v}_{0}. The optimal variational choices are furnished by the solutions of the Euler-Lagrange equations

$$\delta E^{v}_{4}/\delta u_{ij}=\delta E^{v}_{4}/\delta q_{ijk}=0\ , \tag{2.17}$$

$$\delta\epsilon^{v}_{0}/\delta u_{Ij}=\delta\epsilon^{v}_{0}/\delta q_{Ijk}=0\ . \tag{2.18}$$

In this paper we use the solutions u_{ij} and u_{Ij} of the approximated Euler-Lagrange equations given in Ref. 12 and the parametrized triplet correlations q_{ijk} adopted by Schmidt *et al.*[22] in a variational Monte Carlo calculation of the binding energy of liquid ^{4}He. This correlation has the form given in Eq. (1.7) with

$$\zeta(r_{ij})=\zeta(r_{Ij})=\begin{cases}\sqrt{\lambda}r\exp\{-[(r-r_t)/\omega_t]^2\} & \\ \qquad\times[(r-r_B)/r_B]^3 & \text{for } r\leq r_B\ , \\ 0 \quad \text{for } r>r_B\ . & \end{cases} \tag{2.19}$$

The values of the parameters $\lambda=7\sigma^{-2}$, $r_t=0.82\sigma$, $\omega_t=0.5\sigma$, and $r_B=\frac{1}{2}(108/\rho_0)^{1/3}$, $\sigma=2.556$ Å, which give[22] the minimum of E^{v}_{4} at $\rho=\rho_0$, have been adopted at all of the densities considered in the calculation. The results obtained for ϵ_0 [using the Jastrow model with triplet correlations (J + T)] in conjunction with the LJ potential are shown by the solid curve ϵ^{v}_{0}(J + T) of Fig. 2, where the experimental curve and the Jastrow results [ϵ^{v}_{0}(J)] are also reported for comparison. Triplet correlations lower ϵ^{v}_{0}(J) from 0.14 to −2.58 K at the experimental equilibrium density, contributing to more than 80% of the difference between ϵ^{v}_{0}(J) and the experimental result of −2.79 K. The flatness of the curve ϵ^{v}_{0}(J + T) with respect to the experimental curve is mainly due to the lack of accuracy in the scaling approximation at higher densities, which is more effective in the calculation of ϵ_0 than in the calculation of $E^{v}_{4}(\rho)$. At $\rho=0.023\,88$ Å^{-3} the result for the ^{4}He chemical potential is −4.13 K, which should be compared with the experimental value of −3.97 K; whereas we find $\epsilon_0(\rho=0.023\,88\ \text{Å}^{-3})=0.40$ K, and experimentally one has 1.17 K. Table I gives the ^{3}He chemical potential ϵ^{v}_{0} is a function of the pressure P. $\epsilon^{v}_{0}(P)$ is in better agreement with experiment than $\epsilon^{v}_{0}(\rho)$, but it is still too flat. However, for densities $\rho\leq 0.023$ Å^{-3}, the approximations used in the calculation should be completely reliable. A somewhat better agreement with the experimental results can be obtained by using the more involved triplet correlation of Ref. 11 and the more realistic Aziz potential.[18]

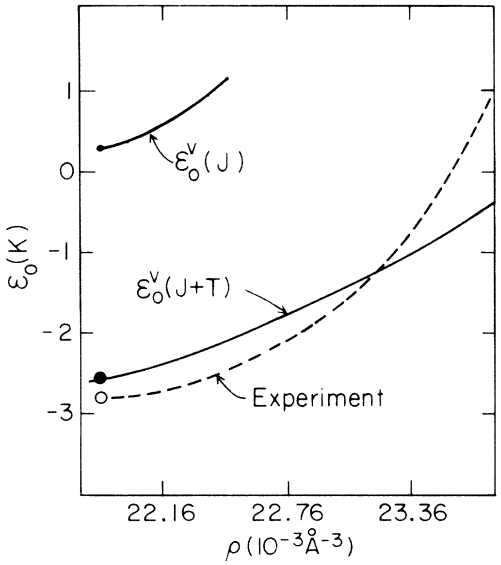

FIG. 2. ^{3}He chemical potential ϵ_0 as a function of the density ρ, calculated with the LJ potential in the Jastrow [ϵ^{v}_{0}(J)] and in the Jastrow + triplet correlation [ϵ^{v}_{0} (J + T)] models and compared with the experimental data (dashed curve). The dots denote the values at the equilibrium density.

B. Excited states

The simplest variational ansatz for the state of one ^{3}He quasiparticle in liquid ^{4}He is given by

$$\Psi_0(\mathbf{p})=|\,\mathbf{p}\rangle=\rho_I(\mathbf{p})\,|\,\Psi_0\rangle\ . \tag{2.20}$$

The expectation value of the Hamiltonian on $|\,\mathbf{p}\rangle$ is easily evaluated by using the relation

$$\frac{\langle\mathbf{p}\,|\,H\,|\,\mathbf{p}\rangle}{\langle\mathbf{p}\,|\,\mathbf{p}\rangle}=E^{v}_{0}+\frac{\langle\Psi_0\,|\,\rho_I(-\mathbf{p})[H,\rho_I(\mathbf{p})]\,|\,\Psi_0\rangle}{\langle\Psi_0\,|\,\Psi_0\rangle}\ , \tag{2.21}$$

where

TABLE I. ^{3}He chemical potential versus pressure for the LJ potential in the Jastrow + triplet correlation model; s is the scaling factor.

P (atm)	ϵ^{v}_{0} (K)	$\epsilon^{\text{expt}}_{0}$ (K)	s
0	−2.62	−2.79	2.36
10	0.14	1.17	2.74
20	2.83	4.69	2.92

$$[H,\rho_I(\mathbf{p})]=\frac{\hbar^2}{2m_3}\rho_I(\mathbf{p})(p^2-2i\mathbf{p}\cdot\nabla_I) . \tag{2.22}$$

The wave function Ψ_0 is real and independent of k; thus the term involving $i\mathbf{p}\cdot\nabla_I$ vanishes and one obtains

$$E_p^v=E_0^v+\frac{\hbar^2p^2}{2m_3} . \tag{2.23}$$

The resulting effective mass $m^*=m_3$ indicates that the wave function $\Psi_0(\mathbf{p})$ of Eq. (2.20) is too simple to describe the single-particle excitations. A better ansatz is given by $\Psi_v(\mathbf{p})$ of Eq. (1.2), which explicitly contains the backflow correlations between the impurity and the ^{4}He atoms. However $\Psi_v(\mathbf{p})$ does not explain the experimental m^* if the Jastrow model is adopted for Ψ_0.[10]

We have calculated the effective mass m^* by using the J + T model previously discussed for Ψ_0 and a backflow correlation operator of the form

TABLE II. Effective mass m^*/m_3, calculated at $\rho_0=0.021\,85$ Å^{-3} for the LJ potential with Jastrow (J) and Jastrow + triplet correlation (J + T) model, and compared with the results of Ref. 10.

	J	J + T	Ref. 10
CA	1.45	1.44	1.58
KSA	1.46	1.44	1.49
HNC/s	1.48	1.46	

$$F_B=\prod_{i=1}^{A}\exp[i\mathbf{p}\cdot\mathbf{r}_{Ii}\eta(r_{Ii})] . \tag{2.24}$$

The expectation value of the Hamiltonian with respect to $\Psi_v(\mathbf{p})$ is given by

$$E_P^{vB}=E_0^v+\frac{\langle\Psi_0\,|\,F_B+\rho_I(-\mathbf{p})[H,\rho_I(\mathbf{p})F_B]\,|\,\Psi_0\rangle}{\langle\Psi_0\,|\,\Psi_0\rangle} . \tag{2.25}$$

Thus, the single-particle excitation energy becomes

$$\epsilon_p^{vB}=\epsilon_0^v+\frac{\hbar^2p^2}{2m_3}\left\{1+\rho\int d\mathbf{r}_{Ij}g_{Ij}(2\eta_{Ij}+\tfrac{2}{3}r_{Ij}\eta'_{Ij}+(m_3/\mu_2)\{\eta_{Ij}^2+\tfrac{1}{3}[r_{Ij}^2(\eta'_{IJ})^2+2\eta_{Ij}r_{Ij}\eta'_{IJ}]\})\right.$$
$$\left.+\rho^2\int d\mathbf{r}_{Ij}\,d\mathbf{r}_{Ik}g_{Ijk}\{\eta_{Ij}\eta_{Ik}+\tfrac{1}{3}[r_{Ij}\eta'_{Ij}\eta'_{Ik}r_{Ik}(\hat{\mathbf{r}}_{Ij}\cdot\hat{\mathbf{r}}_{Ik})^2+2\eta_{Ij}\eta'_{Ik}r_{Ik}]\}\right\} . \tag{2.26}$$

The function $\eta(r)$ adopted in this calculation is of the form

$$\eta(r)=A_0\exp\{-[(r-r_0)/\omega_0]^2\} , \tag{2.27}$$

where the parameters r_0, ω_0, and A_0 are varied to find the minimum of ϵ_p^{vB}. Table II reports the results obtained for the LJ potential at the equilibrium density. The Jastrow and the Jastrow + triplet correlation models give nearly the same results and these are in close agreement with those of Ref. 10. For the sake of comparison we have calculated m^*/m_3 by using the convolution approximation (CA) and the Kirkwood superposition approximation (KSA)[23] for g_{Ijk}. The results are very close to those obtained in HNC/s approximation. The calculated m^*/m_3 is compared with experiment at three different densities in Table III. The comparison confirms the conclusion of Ref. 10 that backflow correlations between the ^{3}He and the ^{4}He atoms are not sufficient to explain the experimental data on m^*/m_3.

III. PERTURBATION THEORY

The variational results discussed in the last section indicate that the eigenfunction of the Hamiltonian

$$|\bar{\Psi}(\mathbf{p})\rangle=\rho_I(\mathbf{p})\,|\,\Psi_0\rangle+\sum_j\alpha_{0j}\,|\,\Psi_j(\mathbf{p})\rangle \tag{3.1}$$

has strong admixtures of CBF states $|\,\Psi_i(\mathbf{p})\rangle$ with $i\neq0$. The CBF scheme[23] is based on the following unperturbed and interaction Hamiltonians:

$$H_{0,ij}=\delta_{ij}\frac{\langle\Psi_i\,|\,H\,|\,\Psi_i\rangle}{\langle\Psi_i\,|\,\Psi_i\rangle}=\delta_{ij}E_i^v , \tag{3.2}$$

$$H_{I,ij}=(1-\delta_{ij})\frac{\langle\Psi_i\,|\,H-E_p\,|\,\Psi_j\rangle}{(\langle\Psi_i\,|\,\Psi_i\rangle\langle\Psi_j\,|\,\Psi_j\rangle)^{1/2}}$$
$$=(1-\delta_{ij})(H_{ij}-E_pN_{ij}) , \tag{3.3}$$

where $E_p=E_0+\epsilon_p$ is the eigenvalue of H for the eigenstate $|\bar{\Psi}(\mathbf{p})\rangle$. The Brillouin-Wigner series for the perturbative correction ΔE_p to E_p^v is given by

TABLE III. The effective mass m^*/m_3 calculated at three different densities for the LJ potential and compared with the experiment. P and P_{expt} are the calculated and experimental pressures. A_0 is one variational parameter of $\eta(r)$. The other two parameters r_0 and ω_0 have been kept fixed at the values $r_0=0.8\sigma$, $\omega_0=0.44\sigma$ given in Ref. 14.

ρ (Å^{-3})	P_{expt} (atm)	P (atm)	$(m^*/m_3)_{\text{expt}}$	(m^*/m_3)	A_0
0.021 85	0	0.1	2.3	1.46	0.23
0.023 88	10	8.0	2.7	1.53	0.26
0.025 71	25	19.4	3.0	1.59	0.26

$$\Delta E_p=\sum_{\alpha(\neq 0)}\frac{(H_{0\alpha}-E_pN_{0\alpha})(H_{\alpha 0}-E_pN_{\alpha 0})}{E_p-E^v_\alpha}+\sum_{\substack{\alpha,\beta(\neq 0)\\(\alpha\neq\beta)}}\frac{(H_{0\alpha}-E_pN_{0\alpha})(H_{\alpha\beta}-E_pN_{\alpha\beta})(H_{\beta 0}-E_pN_{\beta 0})}{(E_p-E^v_\alpha)(E_p-E^v_\beta)}+\cdots , \tag{3.4}$$

where the index refers to the state $|\Psi_0(\mathbf{p})\rangle=\rho_I(\mathbf{p})|\Psi_0\rangle$ and the summations are extended to all of the CBF states defined in Eq. (1.8). The series is first expanded around $\Delta E_0=E_4-E^v_4$ and then resumed in such a way to cancel all the terms which diverge in the thermodynamic limit. This procedure has been devised in Ref. 24 for the ground-state energy of an infinite Fermi system and then generalized in Ref. 19 to calculate the excitation spectrum ϵ_p of one ^{3}He impurity in ^{4}He. Here, we limit ourselves to summarizing the properties of the renormalized CBF perturbative scheme for ϵ_p. The perturbative correction $\delta\epsilon_p$ is given by

$$\delta\epsilon_p=\sum_{\alpha,n_I,n_p}F^{n_I,n_p}_\alpha(\mathbf{p},\delta\epsilon_p) , \tag{3.5}$$

where F^{n_I,n_p}_α is a CBF term having a number n_I of intermediate states and a number n_p of independent phonons. The structure of F is

$$F^{n_I,n_P}_\alpha=\sum_{q_1,\ldots,q_{n_p}}v_{0\alpha_1}v_{\alpha_1\alpha_2}\cdots v_{\alpha_I 0}/D_{\alpha_1}\cdots D_{\alpha_I} , \tag{3.6}$$

where $\alpha_1,\ldots,\alpha_I$ refer to the n_I intermediate states of the αth term, and the sum is extended to all the momenta of the n_p independent phonons. The interaction $v_{\alpha\beta}$ and the energy denominator D_α are given by

$$v_{\alpha\beta}=H_{\alpha\beta}-(E^v_p+\delta\epsilon_p)N_{\alpha\beta} , \tag{3.7}$$

$$D_\alpha=\delta\epsilon_p+\epsilon^v_p-(E^v_\alpha-E^v_0) . \tag{3.8}$$

The sum in Eq. (3.5) is extended to any value of $n_I\geq 1$, $n_p\geq n_I$ and to all of the allowed terms having the same number of intermediate states and of independent phonons.

Both $H_{\alpha\beta}$ and $N_{\alpha\beta}$ in Eqs. (3.7) may have unlinked portions. Their cluster expansion shows up the factorization property expressed by the following two equations:[24]

$$\frac{\langle\Psi_\alpha|\Psi_\beta\rangle}{\langle\Psi_0|\Psi_0\rangle}=\sum_{\substack{\alpha_1,\ldots,\alpha_n\\\beta_1,\ldots,\beta_n}}\prod_i\left[\frac{\langle\Psi_{\alpha_i}|\Psi_{\beta_i}\rangle}{\langle\Psi_0|\Psi_0\rangle}\right]_{\rm NF}+O(1/A) , \tag{3.9}$$

$$\frac{\langle\Psi_\alpha|H-E^v_0|\Psi_\beta\rangle}{\langle\Psi_0|\Psi_0\rangle}=\sum_{\substack{\alpha_i,\ldots,\alpha_n\\\beta_i,\ldots,\beta_n}}\sum_{j=1,n}\left[\frac{\langle\Psi_{\alpha_j}|H-E^v_0|\Psi_{\beta_i}\rangle}{\langle\Psi_0|\Psi_0\rangle}\right]_{\rm NF}\prod_{\substack{i,j=1,n\\(1\neq j)}}\left[\frac{\langle\Psi_{\alpha_i}|\Psi_{\beta_i}\rangle}{\langle\Psi_0|\Psi_0\rangle}\right]_{\rm NF}+O(1/A) , \tag{3.10}$$

where the summations are extended over all possible partitions $\{\alpha_i\}$ and $\{\beta_i\}$ amongst the phonons included in α and β, respectively, such that the total momentum of Ψ_{α_i} is equal to that of Ψ_{β_i} for every $i=1,n$, and the quantity $(X)_{\rm NF}$ represents the sum of the nonfactorizable cluster terms of X. Figure 3 displays a few cluster diagrams of the above matrix elements. Diagram (a) of Fig. 3 belongs to the nonfactorizable part of $\langle\mathbf{k};\mathbf{q}_1|\mathbf{k};\mathbf{q}_1\rangle$ (or $\langle\mathbf{k}|\mathbf{k};\mathbf{q}_1,-\mathbf{q}_1\rangle$) and diagram (b) of Fig. 3 to $\langle\mathbf{k}|\mathbf{k}\rangle\langle 0;\mathbf{q}_1|0;\mathbf{q}_1\rangle$ (or $\langle\mathbf{k}|\mathbf{k}\rangle\langle 0|0;\mathbf{q}_1,-\mathbf{q}_1\rangle$); similarly, diagram (c) of Fig. 3 belongs to the nonfactorizable part of $\langle\mathbf{k};\mathbf{q}_1,\mathbf{q}_2|H-E^v_0|\mathbf{k}+\mathbf{q}_1;\mathbf{q}_2\rangle$ and diagram (d) of Fig. 3 to $\langle\mathbf{k};\mathbf{q}_1|\mathbf{k}+\mathbf{q}_1\rangle\langle 0;\mathbf{q}_2|H-E_0|0;\mathbf{q}_2\rangle$. Each factor $(\langle\Psi_{\alpha_i}|\Psi_{\beta_i}\rangle/\langle\Psi_0|\Psi_0\rangle)_{\rm NF}$ or $(\langle\Psi_{\alpha_i}|H-E^v_0|\Psi_{\beta_i}\rangle/\langle\Psi_0|\Psi_0\rangle)_{\rm NF}$ is of the order A, thus the leading terms in A of the right-hand side (3.9) and (3.10) correspond to partitions having the largest number of states. However, in calculating an interaction term $v_{\alpha\beta}$ appearing in a term F^{n_I,n_p}_α one also has to keep the lower order terms of $\langle\Psi_\alpha|H-E_0|\Psi_\beta\rangle/\langle\Psi_0|\Psi_0\rangle$. In fact, the leading order terms may give rise to an expression which diverges in the thermodynamic limit in which case there is also[19] a counterpart term which cancels it.

In Ref. 19 the terms F^{n_I,n_p}_α were constructed with the interaction $v^*_{\alpha\beta}=H_{\alpha\beta}-E^v_\alpha N_{\alpha\beta}=v_{\alpha\beta}-D_\alpha N_{\alpha\beta}$ for $\alpha\neq 0$ in place of $v_{\alpha\beta}$. The reason given there was that the "interactions" $v^*_{\alpha\beta}$ and $N_{\alpha\beta}$ do not depend upon the energy of the impurity or phonon states belonging to both Ψ_α and Ψ_β. Because of this property, their use helps into the understanding of the cancellation process occurring amongst those CBF terms which diverge in the thermo-

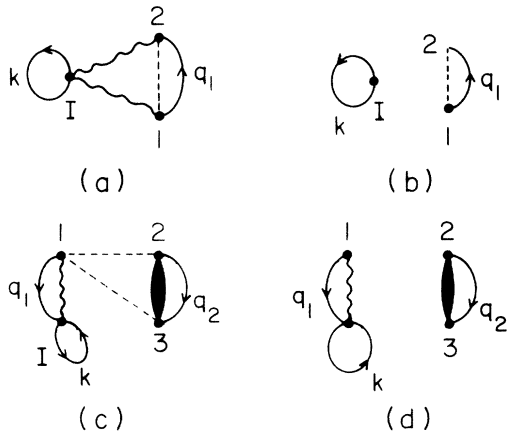

FIG. 3. Cluster diagrams contributing to the CBF matrix elements given in Eqs. (3.9) and (3.10). A thick solid line represents the interaction and a solid q line oriented from i to j denotes $\exp(i\mathbf{q}\cdot\mathbf{r}_{ij})$.

dynamic limit. Here we opt for an easier classification scheme of the various perturbative terms and their diagrammatical representation: $v_{\alpha\beta}$ is the only "interaction" of the scheme and it is diagrammatically denoted by a wavy line. Discontinuous wavy lines represent matrix elements factorized according to Eqs. (3.9) and (3.10). Continuous and discontinuous wavy lines will be referred to as single and broken-wavy lines, respectively. A portion $v_{\alpha\beta}^{(n)}$ of $v_{\alpha\beta}$, built up with the n factors corresponding to the partition $\{\alpha_i\}$, $\{\beta_i\}$, $i=1,n$, is given by

$$v_{\alpha\beta}^{(n)}=\sum_{j=1,n}(H_{\alpha_j\beta_j}-E_0^v N_{\alpha_j\beta_j})\prod_{i(\neq j)}N_{\alpha_i\beta_i}-\epsilon_p\prod_{i=1,\ldots,n}N_{\alpha_i\beta_i}\,. \tag{3.11}$$

The energy denominators D_α do not need to be represented, since they are always associated with an intermediate state. A few examples of diagrams are given in Fig. 4. The number of single or broken-wavy lines is equal to n_I+1 and that of separate closed loops to n_p. Diagram (a) of Fig. 4 is a second-order diagram ($n_I=1$) with one independent phonon. Diagrams (d)—(f) of Fig. 4 have $n_I=1$ and two independent phonons. The differences between them arise from the types of terms considered for the $v_{\alpha\beta}$ interactions. Diagram (d) of Fig. 4 is not present in the renormalized perturbative series, since it has been proved[19] that unlinked CBF diagrams cancel amongst themselves. Diagrams (h) and (i) of Fig. 4 are third-order diagrams which have large cancellations with the second-order diagram (g) of Fig. 4 [see the discussion after Eqs. (3.12) and (3.13)], which shows that a classification scheme based upon the number of intermediate states may not be adequate.

For a fixed number n_p of independent phonons, the allowed diagrams are all the possible linked diagrams which are made up of n_p closed loops of vertical, solid, and horizontal wavy lines, with the number of (single or broken) wavy lines being less than or equal to n_p+1. Each wavy lines brings a nondiagonal matrix element $v_{\alpha\beta}$ and an energy denominator D_α (except for the topmost wavy line). Each independent phonon $\mathbf{q}_i$ carries a factor $\Omega/(2\pi)^3$ and an integration over $\mathbf{q}_i$.

In calculating the diagonal and off-diagonal matrix elements we have assumed that the two- and three-particle correlation factors u and q in Ψ_0, are solutions of the Euler equations (2.17) and (2.18). These equations are conveniently written in the following equivalent form:[25]

$$\langle\Psi_0|\prod_{i=1,n}\rho(\mathbf{q}_i)(H-E_0^v)|\Psi_0\rangle=0\,, \tag{3.12}$$

$$\langle\Psi_0|\rho_I(\mathbf{k})\prod_{i=2,n}\rho(\mathbf{q}_i)(H-E_0^v)|\Psi_0\rangle=0\,, \tag{3.13}$$

where the values $n=2,3$ correspond to the Euler equations for the two- or three-particle correlation functions, respectively. The Euler-Lagrange prescription for Ψ_0 ensures the correct linear behavior of the phonon energies at small momenta. Moreover, the use of Eqs. (3.12) and (3.13) leads to considerable simplifications in the calculation of the matrix elements as well as to large cancellations amongst the CBF diagrams. For instance, if Eqs. (3.12) and (3.13) are satisfied for $n=2$, then diagrams (g) and (h) of Fig. 4 cancel each other, while both diagrams (e) and (i) of Fig. 4 give rise to expressions which are linear in $\delta\epsilon_p$ with coefficients which vanish at $p=0$, and, as a consequence, do not contribute to the effective mass m^*/m_3. Similar cancellations are present for all of the diagrams having paired phonon substructures.

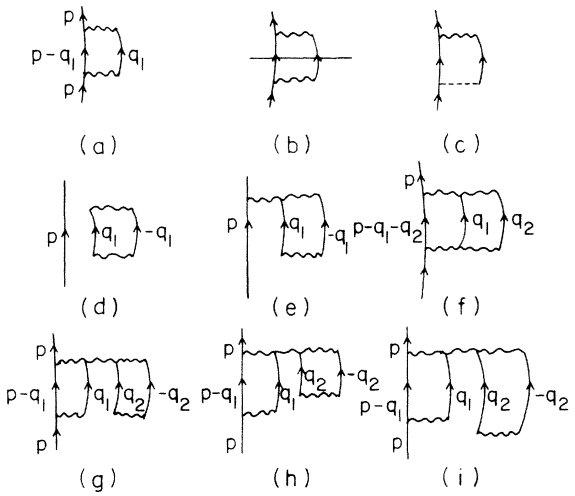

FIG. 4. Examples of allowed and not allowed CBF diagrams. The single and broken wavy lines in diagrams (a) and (d)—(i) represent the interaction, and the oriented solid lines denote impurity (straight line) of phonon (curved line) states. Diagram (d) is unlinked and thus it is not allowed. Diagrams (b) and (c) correspond to diagram (a) in the diagrammatical representation of Ref. 19.

By using the factorization property expressed by Eqs. (3.9) and (3.10), the diagonal matrix elements of the identity operator and of the Hamiltonian are readily calculated

$$\begin{aligned}\langle\mathbf{k};\mathbf{q}_1^{m_1}\mathbf{q}_2^{m_2}\cdots\mathbf{q}_n^{m_n}|\mathbf{k};\mathbf{q}_1^{m_1}\mathbf{q}_2^{m_2}\cdots\mathbf{q}_n^{m_n}\rangle/\langle\Psi_0|\Psi_0\rangle&\\ =\frac{\langle\mathbf{k}|\mathbf{k}\rangle}{\langle\Psi_0|\Psi_0\rangle}\prod_{i=1,n}\frac{\langle 0;\mathbf{q}_i|0;\mathbf{q}_i\rangle^{m_i}}{\langle\Psi_0|\Psi_0\rangle}m_i!+O(1/A)&\\ =\prod_{i=1,n}[AS_2(q_i)]^{m_i}m_i!+O(1/A)&\end{aligned} \tag{3.14}$$

and

$$\begin{aligned}\frac{\langle\mathbf{k};\mathbf{q}_1^{m_1}\cdots\mathbf{q}_n^{m_n}|H|\mathbf{k};\mathbf{q}_1^{m_1}\cdots\mathbf{q}_n^{m_n}\rangle}{\mathbf{k};\mathbf{q}_1^{m_1}\cdots\mathbf{q}_n^{m_n}|\mathbf{k};\mathbf{q}_1^{m_1}\cdots\mathbf{q}_n^{m_n}\rangle}&\\ =E_0^v+\epsilon_k^v+\Sigma\omega^v(q_i)+O(1/A)\,,&\end{aligned} \tag{3.15}$$

where the n-particle structure functions S_n are defined by

$$S_n(\mathbf{q}_1,\ldots,\mathbf{q}_{n-1})=(1/A)\frac{\langle\Psi_0|\rho^\dagger(\mathbf{q}_1)\cdots\rho^\dagger(\mathbf{q}_{n-1})\rho(\mathbf{q}_1+\cdots\mathbf{q}_{n-1})|\Psi_0\rangle}{\langle\Psi_0|\Psi_0\rangle}\,, \tag{3.16}$$

and the variational energies are given by

$$\epsilon_k^v = \frac{\hbar^2}{2m_3} k^2 , \tag{3.17}$$

$$\omega^v(q) = \frac{\hbar^2}{2m_4} \frac{q^2}{S_2(q)} . \tag{3.18}$$

The nondiagonal matrix elements are most conveniently calculated by using Eqs. (3.12) and (3.13), as schematically shown below:

$$\begin{aligned} \langle \mathbf{p}-\mathbf{q}_1-\mathbf{q}_2;\mathbf{q}_1,\mathbf{q}_2 \mid H-E_0^v \mid \mathbf{p} \rangle &= \langle \Psi_0 \mid \rho_I^\dagger(\mathbf{p}-\mathbf{q}_1-\mathbf{q}_2)\rho^\dagger(\mathbf{q}_1)\rho^\dagger(\mathbf{q}_2)[H,\rho_I(\mathbf{p})] \mid \Psi_0 \rangle \\ &= (\hbar^2/2m_3)[p^2-\mathbf{p}\cdot(\mathbf{q}_1+\mathbf{q}_2)]S_3^I(\mathbf{q}_1,\mathbf{q}_2) , \end{aligned} \tag{3.19}$$

where we have used Eq. (2.22) for the commutator.

The mixed n-particle structure functions S_n^I are defined by

$$S_n^I(\mathbf{q}_1,\mathbf{q}_2,\ldots,\mathbf{q}_{n-1}) = \frac{\langle \Psi_0 \mid \rho^\dagger(\mathbf{q}_1)\cdots\rho^\dagger(\mathbf{q}_{n-1})\rho_I(\mathbf{q}_1^\dagger\cdots+\mathbf{q}_{n-1}) \mid \Psi_0 \rangle}{\langle \Psi_0 \mid \Psi_0 \rangle} . \tag{3.20}$$

By using Eq. (3.19) one gets the following expression for diagram (f) of Fig. 4:

$$F_{4(f)}^{1,2} = \frac{\hbar^2}{2m_3} \frac{1}{(2\pi)^3\rho} \int d\mathbf{q}_1 d\mathbf{q}_2 \frac{[\mathbf{p}\cdot(\mathbf{q}_1+\mathbf{q}_2)+\delta\epsilon_p]^2[S_3^I(\mathbf{q}_1,\mathbf{q}_2)]^2}{\delta\epsilon_p+\epsilon_p^v-\epsilon_{\mathbf{p}-\mathbf{q}_1-\mathbf{q}_2}^v-\omega^v(q_1)-\omega^v(q_2)} . \tag{3.21}$$

More generally, a diagram with a number n_p of independent phonon states involves at most the n_p-particle structure functions. Since S_n and S_n^I for $n>2$ contain long-ranged terms, the contribution of a diagram with $n_p>2$ may be large. It is necessary to sum up all the diagrams having the same number of independent phonons, because they cancel each other to a large extent. This is due to the fact that CBF intermediate states are not mutually orthogonal. For instance, the state $|\mathbf{k}-\mathbf{q}_1-\mathbf{q}_2;\mathbf{q}_1,\mathbf{q}_2\rangle$ has a nonvanishing admixture of the state $|\mathbf{k}-\mathbf{q}_1-\mathbf{q}_2;\mathbf{q}_1+\mathbf{q}_2\rangle$. The spurious contributions from the various diagrams with the same n_p cancel when they are all summed up.

For this reason we classify the perturbative terms contributing to $\delta\epsilon_p$ according to the number of the independent phonons considered. Accordingly,

$$\delta\epsilon_p = \sum_{n_p} \delta\epsilon_p^{(n_p)} , \tag{3.22}$$

with

$$\delta\epsilon_p^{(n_p)} = \sum_{\alpha, n_I(\le n_p)} F_\alpha^{n_I,n_p}(\mathbf{p},\delta\epsilon_p^{(n_p)}) , \tag{3.23}$$

where the summation over α is extended to all of the allowed terms (diagrams) with a given n_I and n_p. The dependence of F on $\delta\epsilon_p$ implies a self-consistent solution of Eq. (3.23). Such a solution is not necessary to compute the effective mass, which is indeed given by

$$(m^*/m_3)^{-1} = 1 + \frac{(m/\hbar^2)\frac{1}{p}\sum \frac{\partial F}{\partial_p}(p,0) \mid_{p=0}}{1-\sum \frac{\partial F}{\partial \delta\epsilon_p}(0,\delta\epsilon_p) \mid_{\delta\epsilon_p=0}} . \tag{3.24}$$

IV. PERTURBATIVE CALCULATIONS

In this section we calculate the effective mass m^*/m_3 by using the perturbative scheme described in Sec. III. The diagrams included in the calculation are displayed in Fig. 5 and correspond to all of the contributing OIP and TIP diagrams. In addition, we have calculated the contribution from all of the ladder-type diagrams [(a) and (b) of Fig. 5 are the first two diagrams of the ladder series], in

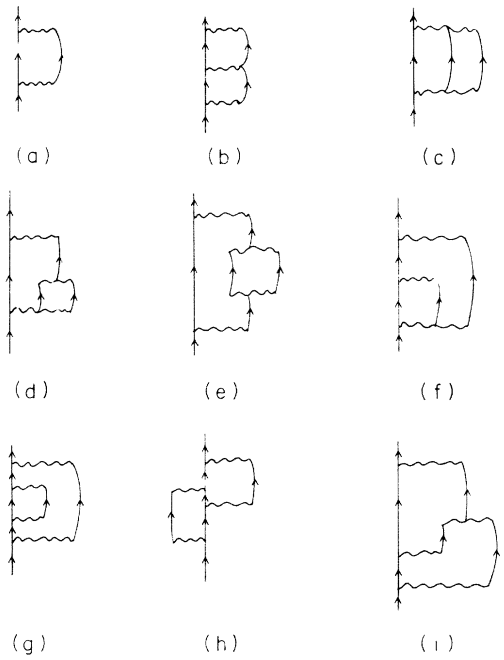

FIG. 5. OIP and TIP diagrams included in the calculation of the effective mass of one ^{3}He impurity in ^{4}He.

order to check the convergence in the number of independent phonons.

The ingredients necessary to calculate the above perturbative contributions are the two- and three-particle structure functions. The structure functions S_2 and S_2^I used are those obtained in the variational calculation of the chemical potential ϵ_0^v and described in Sec. II. The three-particle structure functions S_3 and S_3^I have been calculated by using the convolution approximation (CA), the Kirkwood superposition approximation (KSA) and the HNC/s approximation. S_3^I is readily extracted from Eq. (3.20) with the result

$$S_3^I(\mathbf{q}_1,\mathbf{q}_2)=S_2^I(\mathbf{q}_1+\mathbf{q}_2)[S_2(q_1)+S_2(q_2)-2] +S^I(q_1)S^I(q_2)+\Delta S^I(\mathbf{q}_1,\mathbf{q}_2) , \quad (4.1)$$

where the remainder $\Delta S^I(\mathbf{q}_1,\mathbf{q}_2)$ is given by

$$\Delta S^I(\mathbf{q}_1,\mathbf{q}_2)=\rho^2\int d\mathbf{r}_{Ij}\,d\mathbf{r}_{Ik}[h_{Ij}h_{Ik}h_{jk}+g_{Ij}g_{Ik}g_{jk} \times(e^{q_{Ijk}+A_{Ijk}}-1)] \times\exp(i\mathbf{q}_1\cdot\mathbf{r}_{Ij}+i\mathbf{q}_2\cdot\mathbf{r}_{Ik}) , \quad (4.2)$$

with $h=g-1$. The three different approximations used correspond to the following expressions for ΔS^I:

$$\Delta S^I_{\mathrm{CA}}(\mathbf{q}_1,\mathbf{q}_2)=S_2^I(\mathbf{q}_1+\mathbf{q}_2)[S_2(q_1)-1][S_2(q_2)-1] , \quad (4.3)$$

$$\Delta S^I_{\mathrm{KSA}}(\mathbf{q}_1,\mathbf{q}_2)=\rho^2\int d\mathbf{r}_{Ij}\,d\mathbf{r}_{Ik}h_{Ij}h_{Ik}h_{jk} \times\exp(i\mathbf{q}_1\cdot\mathbf{r}_{Ij}+i\mathbf{q}_2\cdot\mathbf{r}_{Ik}) , \quad (4.4)$$

$$\Delta S^I_{\mathrm{HNC}/s}(\mathbf{q}_1,\mathbf{q}_2)=\Delta S^I_{\mathrm{KSA}}(\mathbf{q}_1,\mathbf{q}_2) +\rho^2\int d\mathbf{r}_{Ij}\,d\mathbf{r}_{Ik}g_{Ij}g_{Ik}g_{jk} \times(1+s/2)A^J_{4,Ijk} \times\exp(i\mathbf{q}_1\cdot\mathbf{r}_{Ij}+i\mathbf{q}_2\cdot\mathbf{r}_{Ik}) , \quad (4.5)$$

where the scaling factor s is taken from the variational calculations of Sec. II. In Eq. (4.5) $A^J_{4,Ijk}$ refers to the four-particle Abe diagram, which in the present calculation is computed without triplet correlations. Similarly, $S_3(\mathbf{q}_1,\mathbf{q}_2)$ is obtained from Eqs. (4.1)—(4.5) by first replacing $S_2^I(\mathbf{q}_1+\mathbf{q}_2)$ with $S(\mathbf{q}_1+\mathbf{q}_2)-1$, then dropping the upper index I, and finally substituting particle i for particle I.

The contribution to m_3/m^* from ladder diagrams is given by

$$\delta_L(m_3/m^*)=[1/(2\pi)^3\rho]^3\tfrac{1}{3}\int d\mathbf{q}_1\,d\mathbf{q}_2\frac{(\mathbf{q}_1\cdot\mathbf{q}_2)}{E^{1/2}(q_1)E^{1/2}(q_2)}\frac{S_2^I(q_1)}{S^{1/2}(q_1)}\frac{S_2^I(q_2)}{S^{1/2}(q_2)}[-\rho\delta(\mathbf{q}_1-\mathbf{q}_2)+L(\mathbf{q}_1,\mathbf{q}_2)] , \quad (4.6)$$

where

$$E(q)=q^2+(m_3/m_4)q^2/S_2(q) . \quad (4.7)$$

The function $L(\mathbf{q}_1,\mathbf{q}_2)$ is the solution of the following integral equation:

$$L(\mathbf{q}_1,\mathbf{q}_2)=L_0(\mathbf{q}_1,\mathbf{q}_2)-\frac{1}{(2\pi)^3\rho}\int d\mathbf{q}L(\mathbf{q}_1,\mathbf{q})L_0(\mathbf{q},\mathbf{q}_2) , \quad (4.8)$$

where

$$L_0(\mathbf{q}_1,\mathbf{q}_2)=\frac{\mathbf{q}_1\cdot\mathbf{q}_2}{[E(q_1)S(q_1)]^{1/2}[E(q_2)S(q_2)]^{1/2}} \times[S_3^I(\mathbf{q}_1,\mathbf{q}_2)+(m_3/m_4)S_2^I(\mathbf{q}_1+\mathbf{q}_2)] . \quad (4.9)$$

Diagrams (a) and (b) of Fig. 5 are given by the integral in Eq. (4.6), when only the δ function or the function $L=L_0$ is retained in the expression enclosed in the second set of square brackets.

The results obtained for the LJ potential are given in Table IV. The first two columns report the OIP- and TIP-ladder contributions and the third column lists the results from all of the ladder diagrams with more than two independent phonons. The results depend very little on the approximation used for the three-particle structure function S_3^I, indicating that the CA is already good enough to compute ladder diagrams. The convergence in the number of independent phonons is very fast, suggesting that the OIP + TIP approximation might be a good approximation for the complete set of diagrams also. The OIP results obtained for the effective mass m^*/m_3 are very close to the variational results reported in Table II, which confirms that perturbative corrections calculated with one-phonon intermediate states only, correspond[15,16] to the backflow correlations. The contributions to m_3/m^* from TIP diagrams (c)—(i) of Fig. 5 are calculat-

TABLE IV. Perturbative contributions to $\delta(m_3/m^*)$ from ladder diagrams at three different densities for the LJ potential. The last column reports the effective mass resulting from the summation of all the ladder terms.

ρ (Å^{-3})		OIP	TIP	nIP ($n>2$)	m^*/m_3
0.021 85	CA	−0.42	0.10	−0.03	1.54
	KSA	−0.42	0.09		
0.023 88	CA	−0.46	0.13	−0.04	1.59
	KSA	−0.46	0.12		
0.025 71	CA	−0.50	0.17	−0.06	1.63
	KSA	−0.50	0.16		

TABLE V. Analysis of perturbative contributions to $\delta(m_3/m^*)$ from all the diagrams with two independent phonons, at equilibrium density and for the LJ potential.

	CA	KSA	HNC/s
OIP	−0.42	−0.42	−0.42
$(TIP)_2$	0.16	0.16	0.16
$(TIP)_3$	−0.13	−0.26	−0.22
TIP	0.03	−0.10	−0.06

TABLE VI. Effective mass m^*/m_3 calculated for the Lennard-Jones and Aziz potentials at the $n_p=1$ order of the perturbative scheme, by adding the $n_p=2$ diagrams, and by adding the ladder diagrams with $n_p \geq 3$.

	0.021 85		0.023 88	0.025 71
ρ (Å^{-3})	Aziz	LJ	LJ	LJ
OIP	1.8	1.7	1.9	2.0
+ TIP	2.1	1.9	2.4	2.5
+ ladders	2.2	2.0	2.6	2.8
Expt.	2.3		2.7	3.0

ed by using the expressions given in the Appendix. The functions $S_3^I(\mathbf{q}_1,\mathbf{q}_2)$ and $S_2^I(\mathbf{q}_1+\mathbf{q}_2)S_3(\mathbf{q}_1,\mathbf{q}_2)$, appearing in most of the terms δ_i, do not vanish in the limit $q_1 \to 0$ or $q_2 \to 0$. This implies that δ_c, δ_d, and δ_e are large compared, for instance, to δ_L. Most of their contribution is spurious and is due to the nonorthogonality of $|\mathbf{k}-\mathbf{q}_1-\mathbf{q}_2;\mathbf{q}_1,\mathbf{q}_2\rangle$ with $|\mathbf{k}-\mathbf{q}_1-\mathbf{q}_2;\mathbf{q}_1+\mathbf{q}_2\rangle$. Such spuriousness is completely removed in the combination $\delta_c+\delta_d+\delta_e$ which in fact is of the same order of δ_L. There are some further important cancellations which have to be taken into account. We extract from the structure function $S_3^I(\mathbf{q}_1,\mathbf{q}_2)$ its factorized part $S_2^I(q_1)S_2^I(q_2)$, namely,

$$S_3^I(\mathbf{q}_1,\mathbf{q}_2)=S_2^I(q_1)S_2^I(q_2)+\tilde{S}_3^I(\mathbf{q}_1,\mathbf{q}_2)\ , \tag{4.10}$$

where

$$\tilde{S}_3^I(\mathbf{q}_1,\mathbf{q}_2)=S_2^I(\mathbf{q}_1+\mathbf{q}_2)[S_2(q_1)+S_2(q_2)-2]+\Delta S^I\ . \tag{4.11}$$

By inserting Eq. (4.10) into the Eqs. (A1) and (A4) of the Appendix the terms $\delta^{(F)}$ arising from the part $S_2^I(q_1)S_2^I(q_2)$ of $S_3^I(\mathbf{q}_1,\mathbf{q}_2)$ cancel between themselves and with δ_g. At equilibrium density and for the LJ potential, $\delta_g=-1.13$, $\delta_c^{(F)}=-1.07$, and $\delta_f^{(F)}=2.27$.

The results obtained by summing up the contributions from all the TIP diagrams are given in Table V. $(TIP)_2$ represents the sum $\delta_b^{(F)}+\delta_c^{(F)}+\delta_f^{(F)}+\delta_g+\delta_h$ of the expressions in which the three-particle structure functions do not enter explicitly; $(TIP)_3$ collects the rest of the contributions and has a strong dependence on the approximations used to calculate S_3 and S_3^I. Since the TIP contribution is $\sim 15\%$ of the OIP contribution, terms with three or more independent phonons are not expected to contribute more than 5% of the OIP contribution. The calculated values of the effective mass are reported in Table VI for both the Aziz potential and LJ potentials. The results obtained when also the ladder diagrams with $n_p>2$ are added to the calculation are expected to be slightly reduced if all the $n_p=3$ diagrams are considered.

The more realistic Aziz potential brings the calculated effective mass at equilibrium density even closer to the experimental value. The satisfactory results obtained strongly support the belief that the OIP + TIP approximation is a reasonably good approximation for calculating the excitation spectrum of one ^{3}He impurity in ^{4}He. The HNC/s approximation used here should include the main contributions coming from the elementary and Abe diagrams to the three-particle structure functions. However, we believe that more extensive analysis of the approximation to be used for S_3 and S_3^I is required in order to check the accuracy of our HNC/s method. In particular, the triplet correlations should be included explicitly through the Abe term in the calculation of ΔS and ΔS^I. Moreover, the use of an optimized triplet correlation like the one recently discussed in Ref. 26 would be desirable both to check the accuracy of the approximations made in applying Eqs. (3.12) and (3.13) for $n=3$ and to determine a better three-body distribution function. Work in this direction is in progress.

The technique developed in this paper allows one also to compute the single-particle spectrum of one ^{3}He impurity in ^{4}He at higher momenta. From such a calculation a better understanding of the behavior of the spectrum around the rotonic ^{4}He minimum should be available.

ACKNOWLEDGMENTS

The authors are very much indebted to V. R. Pandharipande and E. Manousakis for helpful discussions. They acknowledge the Centro Nazionale Universitario di Calcolo Elettronico of Pisa for the assistance in the computing facilities. One of us (A.F.) acknowledges the partial financial support from "Fondazione Angelo della Riccia." The work has been supported in part by a NATO Grant No. 0453/82 and by the U.S. Department of Energy (Division of Material Sciences) by Grant No. DE-AC02-76ER01198.

APPENDIX

In this appendix we give the expressions corresponding to the contributions to m_3/m^* from the TIP diagrams (c)—(i) of Fig. 5:

$$\delta_c=-[1/(2\pi)^3\rho]^2\tfrac{1}{6}\int d\mathbf{q}_1\, d\mathbf{q}_2 \frac{Q^2[S_3^I(\mathbf{q}_1,\mathbf{q}_2)]^2}{E_m S_2(q_1)S_2(q_2)}\ , \tag{A1}$$

$$\delta_d=[1/(2\pi)^3\rho]^{2\frac{1}{3}}\int d\mathbf{q}_1 d\mathbf{q}_2 \frac{Q^2 T_m}{E_m E(Q)} \frac{S_2^I(Q)S_3^I(\mathbf{q}_1,\mathbf{q}_2)}{S_2(q_1)S_2(q_2)S_2(Q)} , \tag{A2}$$

$$\delta_e=-[1/(2\pi)^3\rho]^{2\frac{1}{6}}\int d\mathbf{q}_1 d\mathbf{q}_2 \frac{Q^2}{E_m} \frac{T_m^2}{E(Q)} \frac{[S_2^I(Q)]^2}{S_2(Q)} \frac{1}{S_2(q_1)S_2(q_2)} , \tag{A3}$$

$$\delta_f=[1/(2\pi)^3\rho]^{2\frac{2}{3}}\int d\mathbf{q}_1 d\mathbf{q}_2 \frac{(\mathbf{q}_1\cdot\mathbf{Q})E_1}{E_m E(q_1)} \frac{S_2^I(q_1)S_2^I(q_2)S_3^I(\mathbf{q}_1,\mathbf{q}_2)}{S_2(q_1)S_2(q_2)} , \tag{A4}$$

$$\delta_g=-[1/(2\pi)^3\rho]^{2\frac{1}{3}}\int d\mathbf{q}_1 d\mathbf{q}_2 \frac{q_1^2 E_1^2}{E_m E^2(q_1)} \frac{[S_2^I(q_1)S_2^I(q_2)]^2}{S_2(q_1)S_2(q_2)} , \tag{A5}$$

$$\delta_h=-[1/(2\pi)^3\rho]^{2\frac{1}{3}}\int d\mathbf{q}_1 d\mathbf{q}_2 \frac{(\mathbf{q}_1\cdot\mathbf{q}_2)E_1E_2}{E_m E(q_1)E(q_2)} \frac{[S_2^I(q_1)S_2^I(q_2)]^2}{S_2(q_1)S_2(q_2)} , \tag{A6}$$

$$\delta_i=[1/(2\pi)^3\rho]^{2\frac{2}{3}}\int d\mathbf{q}_1 d\mathbf{q}_2 \frac{(\mathbf{q}_1\cdot\mathbf{Q})E_1 T_m}{E_m E(Q)E(q_1)} \frac{S_2^I(q_1)S_2^I(q_2)S_2^I(Q)}{S_2(q_1)S_2(q_2)S_2(Q)} , \tag{A7}$$

where $\mathbf{Q}=\mathbf{q}_1+\mathbf{q}_2$ and the quantities E and T are given by

$$E_i=E(q_i)+\mathbf{q}_1\cdot\mathbf{q}_2 \quad \text{for } i=1,2 , \tag{A8}$$

$$E_m=E_1+E_2 , \tag{A9}$$

$$T_m=Q^2 S_3(\mathbf{q}_1,\mathbf{q}_2)+(m_3/m_4)\mathbf{Q}\cdot[\mathbf{q}_1 S_2(q_2)+\mathbf{q}_2 S_2(q_1)] . \tag{A10}$$

Diagrams (d), (e), and (i) of Fig. 5 have been counted twice in δ_d, δ_e, δ_i, respectively.

---

*On leave from Dipartimento di Fisica and Istituto Nazionale di Fisica Nucleare, I-56100 Pisa, Italy.

[1]G. Baym, Phys. Rev. Lett. **17**, 952 (1966).
[2]J. Bardeen, G. Baym, and D. Pines, Phys. Rev. **156**, 207 (1967).
[3]L. D. Landau and I. Pomeranchuck, Dokl. Akad. Nauk USSR, **59**, 669 (1948); I. Pomeranchuck, Zh. Eksp. Teor. Fiz. **19**, 42 (1949).
[4]P. Seligman, D. O. Edwards, R. E. Sarwinski, and J. T. Tough, Phys. Rev. **181**, 415 (1969).
[5]A. C. Anderson, W. R. Roach, R. E. Sarwinski, and J. C. Weatley, Phys. Rev. Lett. **16**, 263 (1966).
[6]N. R. Brubaker, D. O. Edwards, R. E. Sarwinski, P. Seligman, and R. A. Sherlock, Phys. Rev. Lett. **25**, 715 (1970).
[7]R. P. Feynman and M. Cohen, Phys. Rev. **102**, 1189 (1956).
[8]T. Burke, K. G. Major, and G. V. Chester, Ann. Phys. (N.Y.) **42**, 144 (1967).
[9]V. R. Pandharipande and N. Itoh, Phys. Rev. A **8**, 2564 (1973).
[10]J. C. Owen, Phys. Rev. B **23**, 5815 (1981).
[11]Q. N. Usmani, S. Fantoni, and V. R. Pandharipande, Phys. Rev. B **26**, 6123 (1982).
[12]A. Fabrocini and A. Polls, Phys. Rev. B **30**, 1200 (1984).
[13]Q. N. Usmani, B. Friedman, and V. R. Pandharipande, Phys. Rev. B **25**, 4502 (1982).
[14]E. Manousakis and V. R. Pandharipande, Phys. Rev. B **30**, 5062 (1984).
[15]T. B. Davison and E. Feenberg, Phys. Rev. **178**, 306 (1969).
[16]W. L. McMillan, Phys. Rev. **182**, 299 (1969).
[17]C. W. Woo, H. T. Tan, and W. E. Massey, Phys. Rev. **185**, 287 (1969).
[18]R. Alrichs, P. Penco, and G. Scoles, Chem. Phys. **19**, 119 (1976); R. A. Aziz, V.P.S. Nain, J. S. Carley, W. L. Taylor, and G. T. McConville, J. Chem. Phys. **70**, 4430 (1979).
[19]A. Fabrocini, S. Fantoni, and A. Polls, An. Fis. **A81**, 93 (1985).
[20]A. Fabrocini and A. Polls, Phys. Rev. B **25**, 4533 (1982).
[21]R. Abe, Prog. Theor. Phys. **21**, 421 (1959).
[22]K. Schmidt, M. H. Kalos, M. A. Lee, and G. V. Chester, Phys. Rev. Lett. **45**, 573 (1980).
[23]E. Feenberg, *Theory of Quantum Fluids* (Academic, New York, 1969).
[24]S. Fantoni, Phys. Rev. B **29**, 2544 (1984).
[25]C. E. Campbell, Phys. Lett. **44A**, 471 (1973); C. C. Chang and C. E. Campbell, Phys. Rev. B **15**, 4238 (1977).
[26]E. Krotscheck, Phys. Rev. B **33**, 3158 (1986).